Co-Adaptive Velocity and Position Control of 3-DoFs Prosthesis via Incremental Learning

Dario Di Domenico, Fabio Egle, *Graduate Student Member, IEEE*, Andrea Marinelli, Michele Canepa, Emanuele Gruppioni, Nicoló Boccardo, Matteo Laffranchi, and Claudio Castellini, *Member, IEEE*

***Abstract*— Upper-limb prosthesis control remains challenging in achieving natural and intuitive movements, especially for devices with multiple actuated degrees of freedom (DoFs), often demanding high cognitive effort. Machine learning aids in mapping phantom limb muscle patterns to prosthetic movements, but is limited by the instability of electromyographic signals over time. This study investigates two simultaneous and proportional myocontrol strategies, based on position and velocity, using incremental learning for a 3-DoFs prosthesis, allowing co-adaptation between the system and the user. Six able-bodied and five limb-difference participants performed Target Achievement Control tests over four sessions per control strategy, assessing performance, usability, workload, simultaneity, and proportionality. Results indicate that velocity control consistently outperforms position control in both populations, yielding lower errors, higher success rates and path efficiency, and lower workload. Notably, both control strategies showed significant improvement over time in the able-bodied group, while only position control improved significantly in the limb-difference group. Interestingly, no significant difference in usability was observed between the two strategies in either group. Position control promoted greater simultaneous actuation of multi-DoFs. However, the overall findings support the use of velocity-based control as a means to improve prosthetic performance and user satisfaction.**

***Index Terms*— Myocontrol, co-adaptation, incremental learning, prostheses, rehabilitation.**

Received 7 August 2025; revised 29 December 2025; accepted 16 January 2026. Date of publication 23 January 2026; date of current version 6 February 2026. This work was supported in part by the Istituto Nazionale per l'Assicurazione contro gli Infortuni sul Lavoro (INAIL) under Grant PR19-PAS-P1—iHannes and Grant PR23-PAS-P1—DexterHand; in part by the European Commission's Horizon Europe Framework Program with the Project IntelliMan (AI-Powered Manipulation System for Advanced Robotic Service, Manufacturing and Prosthetics) under Grant 101070136; in part by the German Federal Ministry of Education and Research (BMBF) under the Robotics Institute Germany (RIG); and in part by The Open University Affiliated Research Centre, Istituto Italiano di Tecnologia, The Open University, Milton Keynes, U.K. *(Dario Di Domenico and Fabio Egle contributed equally to this work.) (Corresponding author: Dario Di Domenico.)*

Dario Di Domenico is with the Rehab Technologies Laboratory, Italian Institute of Technology, 16163 Genova, Italy, and also with DET, Polytechnic of Turin, 10129 Turin, Italy (e-mail: dario.didomenico@iit.it).

Fabio Egle is with the AIROB Laboratory, Friedrich-Alexander Universität Erlangen-Nürnberg, 91052 Erlangen, Germany.

Andrea Marinelli and Matteo Laffranchi are with the Rehab Technologies Laboratory, Italian Institute of Technology, 16163 Genoa, Italy.

Michele Canepa and NicolóBoccardo are with the Rehab Technologies Laboratory, Italian Institute of Technology, 16163 Genoa, Italy, and also with The Open University Affiliated Research Centre (ARC@IIT), MK7 6AA Milton Keynes, U.K.

Emanuele Gruppioni is with the Rehab Technologies Laboratory, Italian Institute of Technology, 16163 Genoa, Italy, and also with the INAIL Prosthetic Center, 00144 Vigorso di Budrio, Italy.

Claudio Castellini is with the AIROB Laboratory, Friedrich-Alexander Universität Erlangen-Nürnberg, 91052 Erlangen, Germany, and also with the Institute of Robotics and Mechatronics, German Aerospace Centre (DLR), 91052 Oberpfaffenhofen, Germany.

Digital Object Identifier 10.1109/TNSRE.2026.3657400

I. Introduction

LIMB loss profoundly impacts individuals with limb-differences, reducing quality of life and complicating the interaction with the environment. Prosthetic devices partially restore lost functionalities, thereby mitigating these challenges. In the context of upper limb absence, notable progress has been made in developing multifunctional and multi-actuated prostheses that closely replicate human movements [1]. Despite significant academic advancements in the design and control of upper-limb prosthetic devices, clinical practice still faces high abandonment rates [2], [3]. Several factors underlie this issue, including limited functionality, complex control systems, and lack of comfort [4], underscoring the need for intuitive control of multiple degrees of freedom (DoFs), co-adaptive approaches and enhanced human-machine interaction over time [4], [5], [6], [7].

Upper-limb prostheses have greatly improved the daily lives of individuals with limb loss, driven by increasingly sophisticated devices incorporating cutting-edge technologies [7], [8]. Progress in robotics has led to prosthetic devices with multiple actuated DoFs. However, a major remaining challenge is the lack of suitable, intuitive control systems capable of effectively actuating all available joints in these complex devices [2], [3], [9]. Nowadays, myoelectric prostheses typically rely on dual-site control, measuring antagonist remnant muscle activity with a pair of electromyographic (EMG) sensors to operate one-DoF hand [1]. However, adding multiple grips and wrist functions makes control unnatural and cumbersome with only two inputs. Since simultaneous joint activation can better approximate human motor behavior [10], [11], research over the past two decades has increasingly focused on data-driven approaches to decode human intentions from multi-modal biosignals [7], [12], [13], [14], [15], [16], [17], some of which

© 2026 The Authors. This work is licensed under a Creative Commons Attribution 4.0 License.
For more information, see https://creativecommons.org/licenses/by/4.0/

have transitioned toward commercial use [18], [19]. However, a major challenge is the data distribution shift over time, due to muscle fatigue, electrode shift, and sweating [20], which degrades prediction accuracy. Implanted EMG electrodes have been explored to improve signal quality and long-term reliability [21], [22], but their invasiveness limits applicability outside the laboratory settings. In recent years, incremental myocontrol methods, including supervised classification [23], [24], [25] and regression-based approaches [26], [27], [28], [29], have been employed to mitigate data distribution shifts. Additionally, fully unsupervised incremental approaches leveraging muscle synergy detection [30], [31], [32], as well as paradigms integrating environmental feedback [33], have been explored, among others [34]. Moreover, these models promote co-adaptation between user and device, enhancing their interaction over time [35], [36]. Comparisons between classification and regression approaches show that the latter more effectively compensate for signal variations [5], leading to its selection for this study.

After offline testing of prosthetic control strategies, real-time evaluation was crucial to assess their effectiveness in device actuation, as offline results do not directly translate to real-time performance or clinical outcomes [37], [38]. Additionally, the variability and fluctuation of EMG signals over time is a critical consideration when designing control algorithms [20], [39]. Therefore, it is essential to test these algorithms over extended periods to evaluate their usability in daily life scenarios and limit accuracy degradation over time [24], [28], [29]. Fitts' law has been widely applied in real-time prosthetic control testing, using cursor movements to represent prosthetic actions [40], [41]. However, while this approach provides a highly standardized environment for initial myocontrol evaluation, it may result in a less intuitive visualization and a weakened correspondence between the user's intended movement and the on-screen response. The Target Achievement Control (TAC) test has been widely adopted to validate control performance of upper limb prostheses in virtual reality environments [26], [42]. Furthermore, extended reality methods have been used to facilitate virtual myocontrol training, enabling users become familiar with prosthesis control. While users show improved performance in serious myogames [43] and achieve greater separability in EMG patterns [44], the transfer of learned skills was effective only when training occurs in virtual environments closely resembling the actual tasks [43], [45]. Thus, virtual training should accurately replicate activities of daily living (ADLs) to facilitate skill transfer [43], [44], [46], [47]. Although the TAC test used in this study does not replicate ADL scenarios, it provides a reproducible framework to assess simultaneous and proportional control of a 3 DoFs prosthesis. In this regard, it offers an intermediate step between 2D control paradigms such as Fitts' law tests [40], [41], and more immersive ADL-based assessments. Future studies should incorporate ADL tasks to further investigate the real-world applicability of myoelectric control strategies.

Both position- and velocity-based control approaches have been investigated for generating actuation commands in prosthetic systems. Motor neuroscience suggests that the nervous system may encode motor commands in terms of velocity [48], while position-based commands align more with the natural encoding scheme of the hand [49], [50]. It remains unclear which strategy is functionally superior or preferred by users. Velocity-based control is commonly used in myoelectric upper-limb prostheses. Despite differing from the natural limb behavior, it leverages non-backdrivability of the motors to maintain hand posture by simply relaxing the muscles. Indeed, no continuous effort is needed to hold onto objects once they are grasped. Comparisons using cursor-control tasks show improved performance with velocity-based control [51], where users adopted a *pulsing* strategy [51], performing small muscle contractions to move the cursor incrementally, followed by pauses for precise task completion [52].

Furthermore, position-type and force/velocity-type myoelectric training and control paradigms have been investigated in multi-DoF settings. Comparisons of force- versus position-targeted inputs for simultaneous control of three wrist DoFs show that force-based training generally yields higher estimation accuracy and improved real-time performance, unless position-based training matches contraction levels [53], [54]. Conventional amplitude-based direct control has been contrasted with sequential and simultaneous pattern-recognition schemes, indicating that direct control is efficient for single-DoF tasks, whereas pattern-recognition strategies improve throughput for multiple active DoFs [40]. A modified Kalman filter has been used to provide proportional position or velocity control of up to six DoFs of the LUKE arm, revealing user- and joint-specific preferences for position versus velocity control modes [55]. Overall, these findings indicate that myoelectric signals can support both position- and velocity-based control of multi-articulate prostheses, with performance depending on control mode, training paradigm, and task demands.

This paper presents a comparative analysis of position- and velocity-based control strategies for actuating a simulated 3-DoFs Hannes upper-limb prosthesis [56], [57], employing an incremental learning approach for rapid model updates based on user inputs. Real-time TAC tests with six able-bodied individuals and five limb-difference participants demonstrated enhanced controllability over time. Since users could simultaneously control multiple DoFs of the prosthetic device, we quantified their concurrent actuation during the TAC tests. Correlations between TAC objective metrics and subjective NASA Task Load Index (NASA-TLX) and System Usability Scale (SUS) assessments highlighted progressive improvement and evidence of co-adaptation between the user and the device. To address the limitations of short-term studies, we conducted experiments across multiple sessions for each control strategy. Furthermore, the resulting dataset from both participant groups is publicly available to the research community.[1]

II. Materials and Methods

A. Experimental Setup and Protocol

This study includes two distinct groups: the able-bodied (AB) population, comprising six participants (26.5 ± 2.6yo,

[1]The data are available on Zenodo for preview at this private link with the following pre-registered DOI: 10.5281/zenodo.14198914.

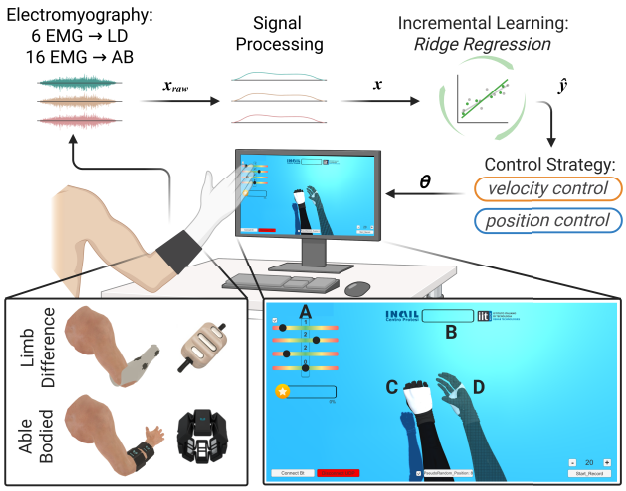


Fig. 1. Experimental setup used for Target Achievement Control tests. Wearable device and Host-PC communication via Bluetooth. Muscle activity is measured using two setups: Two MyoArmbands (16 EMGs) for AB participants and 6 bipolar Ottobock electrodes for the LD population. The control action for the prosthesis is synthesized on the Host PC, where the Unity application for the Target Achievement Control Test (TAC) trials. Participants view the simulated prosthesis on-screen and attempt to match its configuration (C) to a displayed target configuration (&) within a 20-second window. A two-second filling bar (B) activates only when all DoFs are within their respective tolerance ranges simultaneously, indicating a successful trial. Real-time error feedback for each DoF (A) assists participants in determining whether all DoFs are within tolerance ranges.

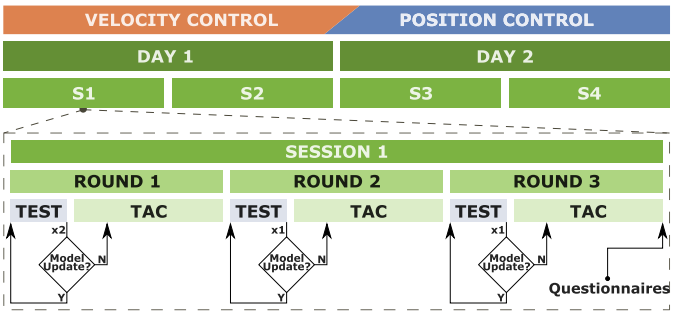


Fig. 2. Experimental protocol of the performed tests. Each type of control strategy (position- and velocity-based) was tested in four sessions (S_1-S_4) over two days, with odd sessions in the morning and even sessions in the afternoon. Each session included three rounds: initial algorithm testing, and in case of subject satisfaction with the prosthesis controllability, the Target Achievement Control (TAC) test was performed. At the end of each session, two questionnaires were provided to the subject.

3m/3f), and the limb-difference (LD) population, consisting of five participants (48.2 ± 14.2yo, 4m/1f). The experiments with the AB population were conducted and evaluated at Friedrich-Alexander Universität and were regulated by its ethical committee (No.: 22-275-S). In contrast, the experiments with the LD population took place at IIT and were approved by the ethical committee of Regione Liguria, Italy (Ref.: IIT_REHAB_HT01). Each participant was informed about the study procedure, provided informed consent, and completed the participant information and data privacy form before the start of the study. We captured multiple sEMG signals from the forearms of able-bodied participants using a pair of Myo armbands. However, due to space constraints, this configuration could not be applied to all LD individuals. For these participants, we adopted the Hannes acquisition setup (see Fig. 1). We prioritized using the maximum number of electrodes feasible for each population to obtain more detailed muscle activation data, rather than limiting the setup to the minimum number that could be uniformly applied across all subjects. AB participants wore two Myo armbands (Fig. 1) from Thalmic Labs on the forearm. These devices recorded sEMG at 200 Hz with eight channels each and 8-bit resolution, streaming data via Bluetooth Low Energy to the host PC, where all 16 channels were combined for processing.

In the LD group, we utilized a custom-made socket equipped with six Ottobock bipolar EMG electrodes, with EMG data were recorded at 300Hz and 16-bit resolution. The socket is made of Thermolyn, a semi-rigid material that maintains its original shape while allowing small variations to accommodate changes in muscle volume during contractions. The sockets are custom-made for each participant, ensuring the electrodes are positioned over the areas of maximum muscle contraction, thereby avoiding bony regions. The electrode locations were determined by manual palpation, targeting forearm regions that showed maximal muscle activation during the intended prosthesis control gestures. The sockets are worn at the beginning of each session, mimicking the daily routine of standard prosthesis use, where users regularly don and doff their prostheses. During the study, the AB and LD participants sat in front of a monitor (approximately 50cm away) showing the TAC environment. The participant's elbow was slightly flexed and resting on the table. The TAC environment featured two representations of the simulated Hannes prosthesis: the controlled one (Fig. 1C) and the target one (Fig. 1D). Additionally, a 2-second filling bar (Fig. 1B) was activated when all DoFs concurrently remained within their respective tolerance ranges. Participants had 20 seconds to reach the target position and maintain it within the correct ranges for at least two consecutive seconds. Throughout the trials, the position and error from the target were measured for each DoF and logged. The target position was centered on the tolerance range of each DoF. The set thresholds were: $th_{HOC} = 0.1$, $th_{WPS} = 0.125$, $th_{WFE} = 0.083$ for the velocity control. For the position control, these thresholds were multiplied by a factor of 1.5. These values were empirically defined through pilot testing [26] to ensure users could successfully achieve the target goals. Without expanding the tolerance thresholds users were unable to reach the targets simultaneously across all DoFs. The experiments were conducted on a Windows PC (LD: Intel Core i7 12th Gen CPU, Intel Iris Xe Graphics GPU; AB: Intel Core i7 12 Gen, Nvidia RTX 3090) running the incremental learning pipeline inside the open-source framework MOSAIC [58] and the Unity application for the TAC test. The signal processing and the incremental learning methods (Fig. 1) were identical for both populations, only differing in the sEMG acquisition setup, thus the number of signals. The signal processing consisted of (i) amplification and rectification, (ii) Butterworth low-pass filtering (2^{nd} order, position control: 0.3 Hz, velocity control: 2 Hz), and (iii) sub-sampling at 25 Hz.

The experimental protocol is depicted in Fig. 2, during which we tested the two control strategies (position- and

velocity-based control) across four sessions conducted over two days per strategy. Two sessions were carried out each day, with consecutive days assigned to the same control strategy. After one week, participants repeated the experiments over another two days (two sessions per day) using the other control strategy. The order of the two control strategies was alternated across participant groups, with one group starting with one strategy and the other beginning with the alternative, to minimize order, practice, and bias effects. Additionally, each session (S_i) comprised three rounds of TAC trials and, ended with the administration of the SUS and NASA-TLX questionnaires. At the beginning of each round (R_j) the participant could freely test the control for 2 min approximately, before deciding whether to update the control model or not (two updates were possible in S_1R_1 of both controls). In case of an update request, an additional 3 s of EMG data for each control action were added to the model incrementally to update the incremental learning algorithm on the new data distribution. Afterward, the participant performed the TAC test, consisting of 21 trials for each round. Therefore, each participant was asked to reach a total of 504 randomly generated prosthesis configurations over the course of eight sessions.

B. Control Command Synthesis

In this study, the Ridge Regression method [59] is employed to obtain a prediction $\hat{\boldsymbol{y}}$ for every observation $\boldsymbol{x} \in \mathbb{R}^m$. The formula is $\hat{\boldsymbol{y}} = W^T\boldsymbol{x}$, with the regression weights $W \in R^{m\times d}$, where $m \in \{16, 6\}$ is the number of sEMG channels for AB and LD, respectively, and $d \in \{5, 7\}$ is the number of necessary actions for the selected control algorithm (i.e., position and velocity control, respectively). The incremental formulation of this method has already been used in prior studies in the area of myoelectric control [26], [27], [28], [29] and utilizes the update of the regression weights W by a new observation $\boldsymbol{x}$ and a label $\boldsymbol{y} \in R^d$ through the Sherman-Morrison formula [60]. For a detailed explanation of the update formulation, readers are directed to the relevant work in the literature [27].

In this study, we compare two control paradigms based on RR: position and velocity control. Both paradigms utilize the RR algorithm's predictions ($\hat{\boldsymbol{y}}$) to generate reference signals for actuating the virtual Hannes prosthesis in a proportional and simultaneous manner. Position-based control acts as a regressor, where RR predictions ($\hat{\boldsymbol{y}}$) are converted into reference positions within the range of motion for each actuated DoF. When the user relaxes their forearm muscles, the prosthesis returns to its default resting position: the hand fully open, the wrist fully supinated, and aligned at the neutral point of the flexion–extension range. This requires the user to maintain continuous muscle contraction to hold a specific configuration, similar to how we naturally keep muscles engaged to prevent dropping an object. In this case, five control actions ($d = 5$) were trained: hand closing (C), wrist pronation (P), wrist flexion (F), wrist extension (E), and resting (R). Muscle relaxation facilitated opposite movements, such as hand opening and wrist supination, with pilot tests showing intuitive use of the resting state for hand opening (O) and wrist supination (S). To calculate the position values for position control, predictions for each action ($\hat{y}_i$) are clipped between 0 and 1, yielding corrected predictions ($\bar{y}_i$). Therefore, the clipped control values (θ in Fig. 1) for hand opening/closing (HOC), wrist flexion/extension (WFE), and wrist pronation/supination (WPS) at control timestep n are then computed as follows:

$$\begin{aligned}\theta_{HOC,n} &= \bar{y}_{C,n}\\ \theta_{WPS,n} &= 1 - \bar{y}_{P,n}\\ \theta_{WFE,n} &= \frac{\bar{y}_{E,n} - \bar{y}_{F,n} + 1}{2}\end{aligned} \tag{1}$$

As for velocity control, it also uses RR predictions but maps them to discrete step values for each actuated DoF. These step values are added or subtracted from the current DoF position, allowing the user to maintain the current prosthesis configuration even without ongoing muscle contraction. This enables users to hold specific grips without continuous effort, as the motor position remains stable in the absence of new predictions. In this case, seven control actions ($d = 7$) were trained: hand closing (C), hand opening (O), wrist pronation (P), wrist supination (S), wrist flexion (F), wrist extension (E), and resting (R), accounting for both directions of movement for each actuated DoF of the Hannes prosthesis. The resting state corresponds to a fixed configuration, allowing users to relax their forearm muscles once a target position is reached. Before calculating the values for velocity control, a deadband is subtracted from the predictions $\hat{y}_i$. The deadband $d_b = 0.3$ was chosen to reduce unintended movements during rest. This value was selected based on pilot testing [26] and prior myoelectric control studies [61], [62]. The predictions are then rescaled between 0 and 1 to produce corrected predictions $\bar{y}_i$. The normalized control values (θ in Fig. 1) for HOC, WFE, and WPS ($\theta_{DoF,n}$) are computed as follows:

$$\theta_{DoF,n} = \begin{cases}\theta_{DoF,n-1} + d_s \cdot (\bar{y}_{k,n} - \bar{y}_{j,n}) & \text{if}(\hat{y}_{k,n} \geq d_b \wedge \hat{y}_{j,n} \geq d_b)\\ \theta_{DoF,n-1}, & \text{otherwise}\end{cases} \tag{2}$$

In this case, k represents C, S, and E movements, while j represents O, P, and F, with a scaling factor ($d_s = 4$) chosen to match the virtual prosthesis's movement speed to that of the real Hannes hand.

C. Simultaneity and Proportionality Assessment

In addition to the evaluation of prosthetic control performance via the TAC test metrics, particular emphasis was placed on the simultaneous actuation of multi-DoFs. Both position and velocity control methods allowed simultaneous and proportional control over three DoFs. Since some participants had incomplete prediction logs from the incremental learning algorithm, we randomly selected an equal number of logged predictions ($n_p = 2 \times 10^4$) across users and control methods to ensure a balanced dataset. The logging of model predictions had no impact on the metrics derived from TAC data, which were independently recorded in a separate application. We computed the simultaneous control spaces, i.e., joint position and joint velocity (see Fig. 3), based on the corrected predictions $\bar{y}_i$, as these directly tuned joint actuation and

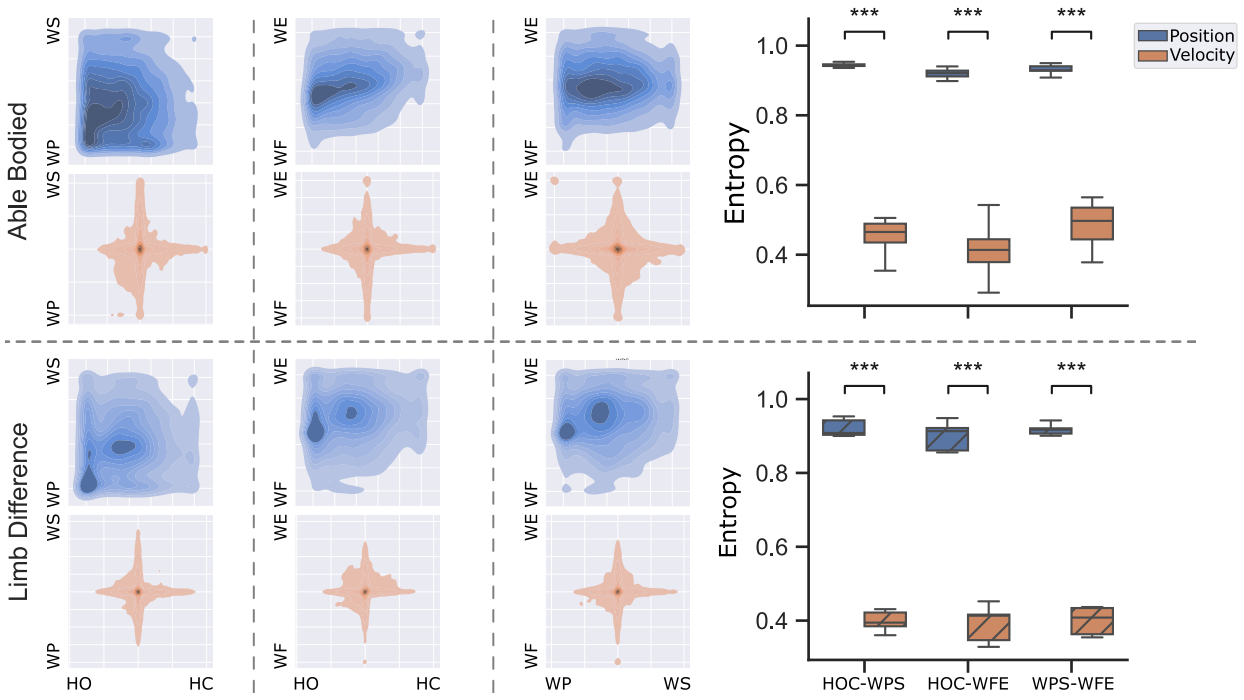


Fig. 3. Quantification of simultaneous multi-joint actuation under position and velocity control strategies. The density plots illustrate the distribution of DoF actuation across two-dimensional joint spaces for AB (top) and LD (bottom) populations. The boxplots depict the entropy index, with median values (horizontal line), 25^{th} and 75^{th} percentiles (box boundaries), and whiskers extending 1.5 times the interquartile range. Outliers were capped. Statistical significance is indicated as ***: $p < 0.001$.

were intuitively controllable through the participant's muscle activation. For position control, the joint position was derived from the corrected predictions which were mapped to each DoF as described in Eq. 1. Regarding the velocity control, the joint velocity was derived from the difference between antagonistic predictions within the same DoF, as defined in Eq. 2 ($\bar{y}_{k,n} - \bar{y}_{j,n}$). To assess simultaneous and proportional control, bi-variate histograms (bins $N_b = 20$) were computed for all combinations of two DoFs. Bin probabilities p_i were determined, and Shannon entropy (H) was calculated as:

$$H = -\sum_{i=1}^{N_b} p_i \log_2 p_i \tag{3}$$

where p_i is the probability of values falling in the i^{th} bin. Entropy was normalized using the maximum entropy $H_{\max} = \log_2 N_b$, yielding normalized entropy $H_{\text{norm}} = \frac{H}{H_{\max}}$. Entropy scores were computed per participant and control, and after validating prerequisites, dependent t-tests were conducted separately for each group (AB, LD) to compare position and velocity control paradigms.

D. Target Achievement Control Test

During the TAC test, we recorded the error between the actual position and the target position for each joint and computed four different scores to assess the performance of the two control strategies. While these scores are computed independently for each actuated DoF, we choose to present them collectively across all DoFs to enhance readability and to provide the overall performance of prosthesis controllability.

Error Rate: computed for each DoF as the difference in percentage between the target position and the last reached position in both success and failure trials (i.e., the last value of the target errors per trial). The combined error is obtained by computing the Euclidean distance of the three individual error rates from each trial, calculated for each DoF.

Success Rate: the trial was counted as a success when the user was able to keep the prosthesis in the target interval of each DoF for 2 s simultaneously. Since successful trials require all DoFs to fall within their respective tolerance ranges simultaneously, the success rate score inherently encompasses the performance of all of them.

Path Efficiency: computed for each DoF as the ratio between the optimal trajectory (an uninterrupted movement toward the target position) and the performed trajectory. The optimal trajectory is derived from the sum of all optimal trajectories for each DoF, whereas the actual performed trajectory is derived from the sum of all performed trajectories for each DoF.

Time to Success: time required to reach the target configuration and successfully complete the trial. The maximum allowed time was 20 s, and trials exceeding it were classified as failures.

E. Questionnaires

Additionally, questionnaires were administered to investigate the subjective perception of the participants. In this study, the NASA-TLX [63] and SUS [64] were employed to investigate the perceived workload and usability, respectively. The first part of NASA-TLX assessed mental, physical, temporal, perceived performance, effort, and frustration factors on visual analog scales (0% very low to 100% very high). In the second part of the NASA-TLX, the participants evaluated

individual factors through a pairwise comparison process. The SUS evaluated the usability of the entire system, including the proposed control and the virtual prosthesis, using a five-point Likert scale.

F. Statistical Analysis of TAC Scores

We investigated the influence of factors such as Session and Control on both objective and subjective scores. The objective metrics (Sec. II-D: *error rate*, *success rate*, *path efficiency*, and *time to success*) were aggregated at the session level, separately for each control condition and participant. The subjective scores (Sec. II-E) needed no further processing as they were administered at the end of each session for both control strategies. Outliers were handled during statistical analysis by capping values below the lower bound ($Q_1 - 1.5 \cdot IQR$) and above the upper bound ($Q_3 + 1.5 \cdot IQR$) at their respective thresholds, thereby reducing the influence of extreme values.

To demonstrate learning ability over time (i.e., across sessions) and the effectiveness of the control strategies, we conducted two distinct analyses: the repeated measures ANOVA (rmANOVA) and, in case of significant results, followed up by post-hoc paired t-tests. We utilized a two-way rmANOVA considering both Sessions and Control strategies as factors. Regarding the paired t-test, we examined all feasible combinations of session pairs within the same control strategy (e.g., $S_{pos,1}$–$S_{pos,2}$, $S_{pos,1}$ - $S_{pos,3}$) and pairs within the same sessions while considering both control strategies (e.g., $S_{pos,1}$–$S_{vel,1}$, $S_{pos,2}$–$S_{vel,2}$) as contrasts. These tests were selected because normality was confirmed for the subsets. Before conducting the rmANOVA, we evaluated the sphericity using Mauchly's sphericity test. When p_{GG} is provided, the sphericity assumption of the rmANOVA is violates and the Greenhouse-Geiser correction is applied. Post-hoc paired t-tests are adjusted with the Benjamini-Hochberg method to control the false discovery rate due to multiple comparisons, reported as p_{BH}.

III. Results

In this section, we present the results for both the able-bodied (AB) and limb-difference (LD) populations, examining two control strategies (position and velocity) used to actuate the simulated 3-DoFs Hannes hand. First, we validated the simultaneous actuation of multiple DoFs through the incremental learning model, which supports concurrent movement across DoFs (Sec. III-A). Furthermore, we present the results from the TAC test, which evaluates prosthetic functionality, and analyze trends in these scores over time to capture co-adaptive behavior (Sec. III-B). Subjective scores obtained from participant questionnaires are also reported, revealing temporal trends (Sec. III-C). Finally, we analyze the correlation between TAC and subjective scores (Sec. III-C).

A. Simultaneity and Proportionality of Multi-DoFs Actuation

During the real-time control of the 3-DoFs prosthesis, participants were instructed to reach a target configuration displayed on the screen as quickly as possible, within a maximum of 20 seconds. Subjects were informed to control multiple DoFs simultaneously and proportionally for both control strategies, as enabled by the adopted incremental learning approach. Consequently, we decided to quantitatively evaluate the extent of simultaneous and proportional multi-DoFs actuation. The analysis indicates that position-based control results in a more dispersed cloud of data points in the joint space, suggesting greater concurrent actuation of multiple DoFs (Fig. 3). This further suggests that position control may more closely resemble human motor strategies, as also indicated by prior works [49], [50]. In contrast, the results for velocity control show that participants intentionally actuated one DoF at a time, despite the control method allowed simultaneous actuation.

The Fig. 3 illustrates the simultaneous and proportional actuation of active joint pairs, namely Hand Opening-Closing (HOC), Wrist Pronation-Supination (WPS), and Wrist Flexion-Extension (WFE). The boxplots highlight the entropy computed from the point cloud of concurrent joint actuation in the joint space, revealing that position-based control leads to higher entropy (i.e., greater simultaneity), whereas velocity-based control relies more on sequential movements. We conducted paired t-test on entropy values derived from position- and velocity-based strategies, revealing significant differences across all joint combinations ($p < 0.001$).

B. Target Achievement Control Test

Based on the TAC data described in Sec. II-D, we assessed real-time prosthesis control performance using four key metrics: *error rate*, *success rate*, *path efficiency*, and *time to success*. We analyzed these metrics using rmANOVA with Session and Control as factors, followed by post-hoc paired t-tests. The results of the rmANOVA are summarized in Table I.

The *error rate* trends are illustrated in Fig. 4. In the AB population, the rmANOVA revealed significant effects for both Session and Control, as well as for their interaction. A clear decreasing trend across sessions was observed in both controls control (Fig. 4A-left), supported by pairwise t-tests ($p < 0.05$) in the case of the velocity control. In the LD group, significant effects were found for Session and Control, but not for their interaction. Here, a significant decrease in error was observed for position control between the first and last sessions (Fig. 4A-right), while no significant change emerged for velocity control. For a broader perspective, Fig. 4B presents the distribution of combined errors across the three actuated DoFs, separately for both populations and control strategies.

For the *success rate* (Fig. 5A), the AB group exhibited significant differences by Session and Control, whereas their interaction was not significant. A progressive increase in success rate was evident across sessions in both controls, confirmed by the t-test analysis. In contrast, the LD group showed significant differences only for Control. No session-related or interaction effects were detected.

Regarding *path efficiency* (Fig. 5B), a consistent contrast emerged between the two control strategies for both populations. Significant differences between velocity- and

TABLE I
RM ANOVA ANALYSIS ON TAC METRICS WITH FACTORS: SESSION, CONTROL AND INTERACTION. *: p_{GG}

TAC metrics	Group	Session			Control			Interaction		
		F	p	η^2	F	p	η^2	F	p	η^2
Error Rate	**AB**	$F_{3,15} = 13.19$	$\mathbf{2 \times 10^{-4}}$	0.41	$F_{1,5} = 40.98$	**0.001**	0.66	$F_{3,15} = 3.50$	**0.042**	0.10
	LD	$F_{3,12} = 6.57$	**0.017** *	0.11	$F_{1,4} = 34.04$	**0.004**	0.695	$F_{3,12} = 1.82$	0.245	0.079
Success Rate	**AB**	$F_{3,15} = 37.89$	$\mathbf{2 \times 10^{-4}}$ *	0.45	$F_{1,5} = 21.24$	**0.006**	0.51	$F_{3,15} = 1.27$	0.320	0.06
	LD	$F_{3,12} = 2.82$	0.084	0.07	$F_{1,4} = 31.41$	**0.005**	0.62	$F_{3,12} = 0.54$	0.662	0.03
Path Efficiency	**AB**	$F_{3,15} = 4.28$	0.073 *	0.01	$F_{1,5} = 50.62$	$\mathbf{9 \times 10^{-4}}$	0.77	$F_{3,15} = 3.41$	0.095 *	0.05
	LD	$F_{3,12} = 3.1$	0.067	0.14	$F_{1,4} = 260.3$	$\mathbf{9 \times 10^{-5}}$	0.92	$F_{3,12} = 0.36$	0.785	0.015
Time to Success	**AB**	$F_{3,15} = 50.10$	$\mathbf{2 \times 10^{-5}}$ *	0.47	$F_{1,5} = 7.29$	**0.043**	0.294	$F_{3,15} = 1.88$	0.225	0.082
	LD	$F_{3,12} = 4.05$	0.059	0.082	$F_{1,4} = 37.34$	**0.004**	0.532	$F_{3,12} = 0.69$	0.578	0.033

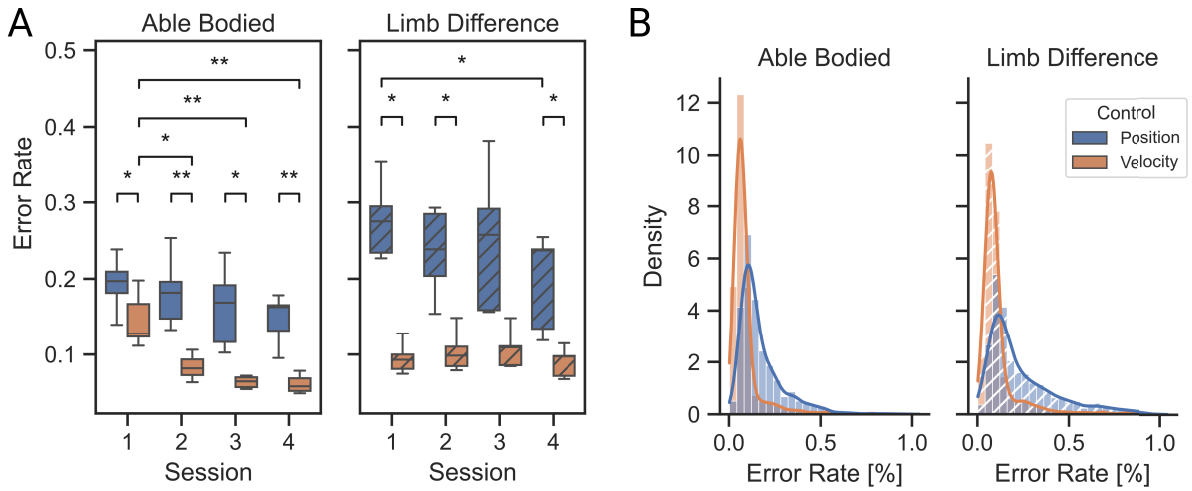


Fig. 4. Error rates. (a): Error Rate for AB (left) and LD (right) populations. The boxplots describe the median value (horizontal line), 25^{th}, and 75^{th} percentiles (extremes of the box). Whiskers extend the interquartile range of 1.5 times, and outliers are capped. *: $p < 0.05$, **: $p < 0.01$. (b): Distributions of the combined error rate in single trials for AB participants (left) and limb-difference ones (right).

TABLE II
RM ANOVA ANALYSIS ON QUESTIONNAIRE RESULTS WITH FACTORS: SESSION, CONTROL AND INTERACTION. *: p_{GG}

Questionnaire	Group	Session			Control			Interaction		
		F	p	η^2	F	p	η^2	F	p	η^2
NASA-TLX	**AB**	$F_{3,15} = 3.33$	0.107 *	0.07	$F_{1,5} = 3.12$	0.137	0.21	$F_{3,15} = 0.34$	0.795	0.01
	LD	$F_{3,12} = 3.45$	0.051	0.10	$F_{1,4} = 80.7$	$\mathbf{9 \times 10^{-4}}$	0.379	$F_{3,12} = 5.84$	**0.033** *	0.18
SUS	**AB**	$F_{3,15} = 10.41$	$\mathbf{6 \times 10^{-4}}$	0.08	$F_{1,5} = 6.49$	0.051	0.16	$F_{3,15} = 1.65$	0.221	0.007
	LD	$F_{3,12} = 1.75$	0.209	0.09	$F_{1,4} = 4.79$	0.094	0.13	$F_{3,12} = 0.66$	0.594	0.03

position-based control were found across all sessions. For AB and LD participants, the rmANOVA reported no significant effect of Session, nor an interaction between Session and Control.

As for *time to success* (Fig. 5C), trends diverged between the two populations. Among AB participants, a significant effect of Session and Control but not the interaction was found. A downward trend in completion time under velocity control was observed, with significant reductions between consecutive sessions ($p < 0.05$), but not controls. In the LD population, both Session and Control had significant effects, while their interaction remained non-significant. Pairwise t-tests identified a significant difference only in session S_2 between the two control conditions.

Participants were allowed to update their control models during each session. The maximum number of updates per control paradigm was 13. On average, AB participants updated 7.33 ± 2.50 times for position and 6.50 ± 1.87 times for velocity control, while LD participants updated 4.80 ± 1.79 and 5.00 ± 2.55 times, respectively, with a decreasing trend over sessions.

C. Questionnaires

In this study, two different subjective scores were administered after each session: the SUS and the NASA-TLX. The results from the rmANOVA are summarised in Table II. The SUS shows different results for the two populations, as represented in Fig. 6A. While the rmANOVA for both populations indicates an influence of the Session factor, they are not significantly influenced. The SUS score of the AB participants was significantly affected by the factor Session, whereas this was not the case for the LD participants. Post-hoc tests revealed no significant difference after BH-correction

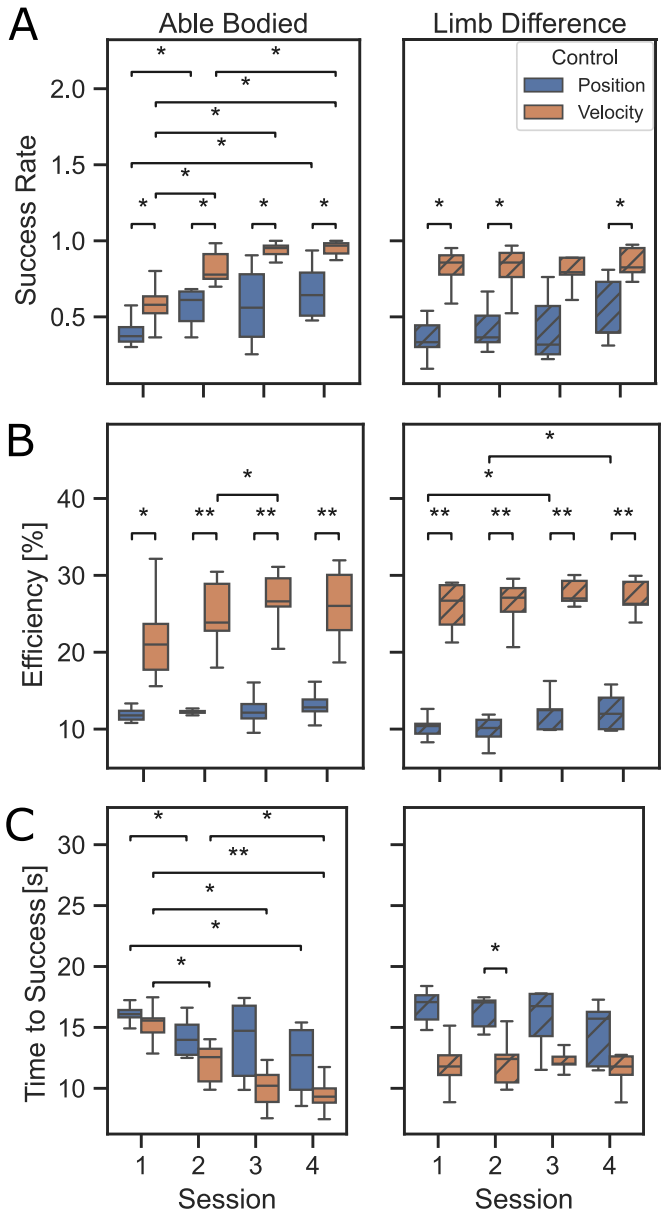


Fig. 5. Success Rate, Path Efficiency and Time to Success. Success Rate (a), Path Efficiency (b) and Time to Success (c) for AB (left) and LD (right) populations. The boxplots describe the median value (horizontal line), 25^{th}, and 75^{th} percentiles (extremes of the box). Whiskers extend the interquartile range by 1.5 times, and outliers are capped. *: $p < 0.05$, **: $p < 0.01$.

for multiple comparisons. The results of the NASA-TLX score are represented in Fig. 6B. Despite a visible downward trend in the AB group, no significant influence of Session and Control could be recognized. The LD population showed a significant influence of the factor Control and the Interaction factor. We conducted post-hoc paired t-tests to compare the two control strategies within the same session and to compare the same control strategy across two different sessions. Fig. 6B reveals a significant difference between $S_{pos,1}$ and $S_{vel,1}$ ($t_4 = 5.54$, $p_{BH} = 0.042$) and $S_{pos,4}$ and $S_{vel,4}$ ($t_4 = 7.30$, $p_{BH} = 0.030$) and between $S_{vel,2}$ and $S_{vel,4}$ ($t_4 = 4.83$, $p_{BH} = 0.045$). Moreover, we present in Fig. 6C-D the aggregated results for all subjects in each population, comparing the first and last sessions to qualitatively highlight changes in the SUS and NASA-TLX scores, with each question being displayed separately. Correlations were conducted on the scores of all participants (LD and AB), examining the relationship between objective metrics that do not require a successful trial (success rate, error rate) and subjective assessments (SUS, NASA-TLX). These objective metrics were selected because they capture the full spectrum of user experience, being computed across both successful and unsuccessful trials, and therefore align more closely with the subjective scores, which asked participants to provide an overall assessment of the entire experiment rather than only the successful attempts. The results of the Spearman correlation are presented in Fig. 7, showing correlation coefficients of $r = 0.49$ and $r = 0.67$ for the success rate, and $r = 0.47$ and $r = 0.64$ for the error rate, corresponding to SUS and NASA-TLX, respectively ($p < 0.001$).

IV. Discussion

To the best of our knowledge, no previous real-time experiment has systematically tested velocity and position approaches for simultaneous and proportional 3-DoFs prosthesis control. Our findings indicate that position control enables more concurrent multi-DoF actuation, implying that it may more closely resemble human motor strategies. In contrast, velocity control primarily actuated one DoF at a time, despite the method allowing simultaneous actuation. This behavior likely stems from position control requiring multiple DoFs to reach a target configuration, whereas velocity control allowed sequential adjustments, with muscle relaxation halting movement at the last reached position. Notably, both strategies enabled simultaneity and proportionality, but position control inherently necessitated it for reaching the target configuration, while the velocity-based one often led to sequential actuation. This pattern is evident in the *Supplementary video*, where the *pulsing* muscle contraction strategy [51], is clearly observed. Therefore, participants using velocity control employed sequential contractions to move the prosthesis' joints in small increments, pausing between movements to refine accuracy. Indeed, a similar behavior could be reproduced with a 3×2 classifier using EMG-based scaling of movement speed if only proportionality were required. However, this approach would have constrained the user to sequential actuation. In our implementation, users were allowed to actuate multiple DoFs simultaneously, yet they often chose not to perform concurrent movements, reflecting their voluntary strategy preferences. Future research should investigate how prolonged use of velocity control influences user behavior regarding simultaneity and proportionality.

To quantitatively evaluate prosthesis controllability, we conducted real-time TAC tests on both AB and LD populations. Since these groups performed the experiments under different conditions, such as variations in EMG acquisition setups and tolerance thresholds, we will discuss the results for each population separately. However, the *error rate* metric derived from the TAC tests remains unaffected by the set tolerance thresholds because the subjects' goal was to get as close as

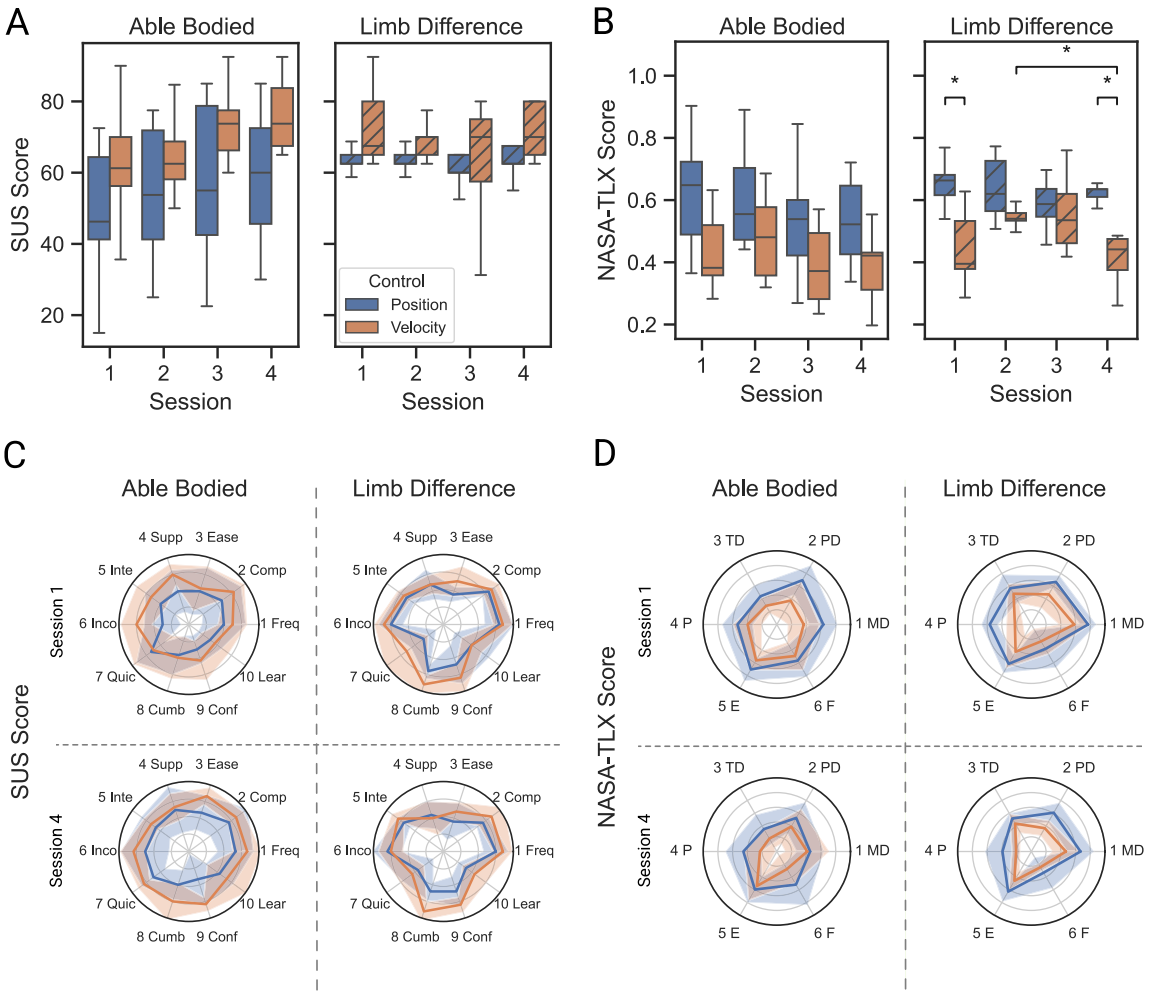


Fig. 6. Subjective scores. The boxplots of (a) SUS and (b) NASA-TLX describe the median value (horizontal line), 25^{th} and 75^{th} percentiles (extremes of the box). Whiskers extend 1.5 times the interquartile range (outliers are capped). *: $p < 0.05$, **: $p < 0.01$. (b): Spider plots in (c) SUS and (d) NASA-TLX illustrate normalized scores across the first and last sessions for AB and LD populations. Radial axis scales: SUS = 0–100; NASA-TLX = 0–1. Mean and SD are represented as marked line and shaded area, respectively. SUS: Frequency of Use (Freq), Complexity (Comp), Ease of Use (Ease), Integration (Inte), Inconsistency (Inco), Quick to Learn (Quic), Cumbersomeness (Cumb), Confidence (Conf), and Learning Effort (Lear). NASA-TLX: The NASA-TLX scores cover: Mental Demand (MD), Physical Demand (PD), Temporal Demand (TD), Performance (P), Effort (E), and Frustration (F).

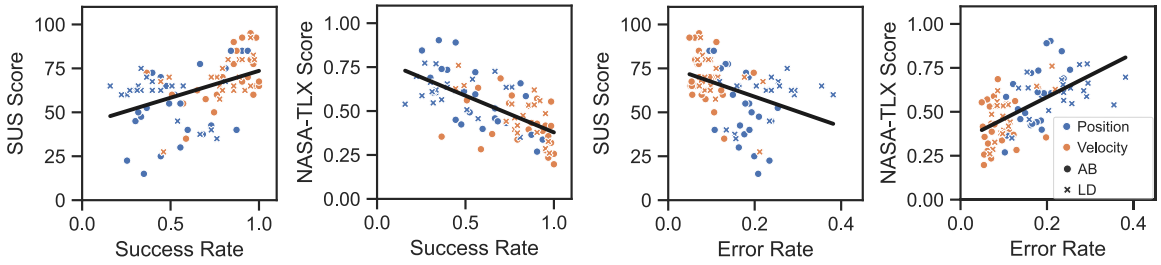


Fig. 7. Questionnaire-TAC scores correlations. This figure shows the relationship between objective (TAC test) and subjective scores (SUS and NASA-TLX questionnaires). The regression lines are only intended to illustrate the overall trend.

possible to the target position rather than simply reaching the tolerance range. Based on this metric depicted in Fig. 4A, the results for AB participants show a decreasing trend over time for both position and velocity control, with the latter yielding better scores. In the LD population, a decreasing error rate was observed for position control, indicating a learning curve over time, while performance remained consistent for velocity control. We hypothesize that the lack of a learning curve in velocity control for the LD group may be due to the prevalence of velocity-based strategies in prosthetic applications, which closely resemble the actuation methods they are accustomed to using. Moreover, we reported the distributions of the error rate separately for the two populations and control strategies in Fig. 4B. We can appreciate the smaller and less spread

errors achieved by both populations when using the velocity control.

As for the *success rate*, we experience a learning curve for velocity control over sessions in the AB population, but no statistical difference occurs in the case of position control, even though the median values for the velocity control within sessions are always greater than the position-based ones. Regarding the LD population, we experience the same trend, where the velocity control results are consistently higher than the position control, confirmed by statistical differences between controls in all session, but S_3.

For the *path efficiency* score, we observe a significant statistical difference across all sessions between velocity and position control. This difference largely stems from the position-based control strategy, which mimics the natural behavior of the hand by returning the prosthesis to a defined resting position when the user is not actively contracting their muscles. This approach requires continuous muscle contraction to maintain the desired configuration. Therefore, small fluctuations in EMG activity lead to slight variations in joint positions, forcing the user to constantly adjust and compensate for these movements, ultimately resulting in a longer overall path. Consequently, the path efficiency score is consistently better with velocity control for both LD and AB populations, highlighting its advantage in minimizing unnecessary movements and improving control precision.

Regarding the *time-to-success* score, which represents the duration required for the user to keep all joints within the tolerance ranges, we observe a decreasing trend over time for the AB population, reflecting the previously mentioned learning curve. Furthermore, the median values for this score are consistently lower for velocity control across sessions for both populations. Overall, the TAC outcomes observed in both LD and AB populations further underscore the superiority of the velocity-based control strategy over the position-based approach in achieving a target position in three actuated DoFs. This is also in line with prior research on prosthetic control [51], [52]. Furthermore, considering the higher measure of simultaneity and proportionality (see Figure 3) for position control, together with its lower path efficiency and higher time to success, suggests an overall reduced movement quality.

The influence of frequency and motivation model updates was not systematically analyzed in this work. However, informal observations suggest that early model updates were aimed at improving control performance, while later ones compensated for session-specific variations, such as electrode shift. The motivations behind self-initiated updates and their impact on long-term control quality should be systematically investigated in future studies.

While the objective scores show a clear picture favoring the velocity control in this TAC study, they are statistically less explicit in this regard. Nevertheless, a trend is also visible between the two controls for the SUS and NASA-TLX. Interestingly, the objective TAC test scores show a strong correlation with the subjective results from the SUS and NASA-TLX questionnaires. As shown in Fig. 7, low error rates correspond to high system usability (SUS) scores and low workload (NASA-TLX) scores. This, in turn, underlines the relationship between the function of the prosthesis and the user's satisfaction. Moreover, we report the results for each question of the two questionnaires separately, over time, and for the two populations (Fig. 6C-D). Indeed, the velocity control consistently falls within the range of position control results for the NASA-TLX. Regarding the SUS, while the overall trend remains similar, this is not observed for every individual question. Additionally, for the SUS, the spider plots exhibit an expansion across sessions, which suggests an improvement in usability. In contrast, the trend for the NASA-TLX shows a gradual constriction over time, indicating a reduction in the perceived effort required throughout the sessions.

During the study, the users had the option to update their models voluntarily. While the effect of the voluntary updates to the method was not directly measured (e.g., by a control group without updates), we expect the incrementality of the approach to play a pivotal role in the stable (or even improving) results over sessions. This is underlined by considering the expected effects of long and tedious assessment sessions and the donning and doffing of the sensors. Therefore, we assume that the incremental nature of the proposed approach, combined with the user's learning effect, fostered co-adaptation, thereby leading to improved overall performance over time, as already demonstrated in previous research [24], [28], [29], [32], [33], [36]. In the future, more studies need to investigate the direct influence of voluntary updates and the fostering of co-adaptation.

In summary, this research supports the integration of velocity-based control strategies in current prosthetics, emphasizing their potential to improve usability and satisfaction for diverse user populations. Future investigations should focus on testing and refining these control strategies during activities of daily living and clinical assessments to evaluate prosthesis performance in real scenarios. It is essential to consider the impact of an embedded system's weight, as well as other pivotal factors such as sweating, electrode shift, muscle fatigue, and limb position effect all of which can significantly influence the controllability of the prosthesis and the overall user experience.

Acknowledgment

The authors would like to thank Dr. Bernhard Weber for his consultation during the initial stages of statistical data analysis. Figure 1 has been created in BioRender. Fabio Egle (2025) (https://BioRender.com/f09d053).

References

[1] A. D. Roche, B. Lakey, I. Mendez, I. Vujaklija, D. Farina, and O. C. Aszmann, "Clinical perspectives in upper limb prostheses: An update," *Current Surg. Rep.*, vol. 7, no. 3, pp. 1–10, Mar. 2019.

[2] E. A. Biddiss and T. T. Chau, "Upper limb prosthesis use and abandonment: A survey of the last 25 years," *Prosthetics Orthotics Int.*, vol. 31, no. 3, pp. 236–257, 2007. [Online]. Available: https://journals.lww.com/poijournal/abstract/2007/31030/upperlimbprosthesisuseandabandonmenta.3.aspx

[3] S. Salminger et al., "Current rates of prosthetic usage in upper-limb amputees–have innovations had an impact on device acceptance?," *Disability Rehabil.*, vol. 44, no. 14, pp. 3708–3713, Jul. 2022. [Online]. Available: https://www.tandfonline.com/doi/full/10.1080/09638288.2020.1866684

[4] P. Capsi-Morales et al., "Functional assessment of current upper limb prostheses: An integrated clinical and technological perspective," *PLoS ONE*, vol. 18, no. 8, Aug. 2023, Art. no. e0289978. [Online]. Available: https://journals.plos.org/plosone/article?id=10.1371/journal.pone.0289978

[5] J. M. Hahne, M. Markovic, and D. Farina, "User adaptation in myoelectric man-machine interfaces," *Sci. Rep.*, vol. 7, no. 1, p. 4437, Jun. 2017. [Online]. Available: https://www.nature.com/articles/s41598-017-04255-x

[6] M. M. Madduri, S. A. Burden, and A. L. Orsborn, "Biosignal-based co-adaptive user-machine interfaces for motor control," *Current Opinion Biomed. Eng.*, vol. 27, Sep. 2023, Art. no. 100462. [Online]. Available: https://www.sciencedirect.com/science/article/pii/S2468451123000181

[7] A. Marinelli et al., "Active upper limb prostheses: A review on current state and upcoming breakthroughs," *Prog. Biomed. Eng.*, vol. 5, no. 1, Jan. 2023, Art. no. 012001, doi: 10.1088/2516-1091/acac57.

[8] H. Huang, L. J. Hargrove, M. Ortiz-Catalan, and J. W. Sensinger, "Integrating upper-limb prostheses with the human body: Technology advances, readiness, and roles in human–prosthesis interaction," *Annu. Rev. Biomed. Eng.*, vol. 26, no. 1, pp. 503–528, Jul. 2024. [Online]. Available: https://www.annualreviews.org/content/journals/10.1146/annurev-bioeng-110222-095816

[9] Z. Chen, H. Min, D. Wang, Z. Xia, F. Sun, and B. Fang, "A review of myoelectric control for prosthetic hand manipulation," *Biomimetics*, vol. 8, no. 3, p. 328, Jul. 2023. [Online]. Available: https://www.mdpi.com/2313-7673/8/3/328

[10] M. Legrand et al., "Simultaneous control of 2DOF upper-limb prosthesis with body compensations-based control: A multiple cases study," *IEEE Trans. Neural Syst. Rehabil. Eng.*, vol. 30, pp. 1745–1754, 2022. [Online]. Available: https://ieeexplore.ieee.org/abstract/document/9805782/

[11] J. M. Hahne, M. A. Schweisfurth, M. Koppe, and D. Farina, "Simultaneous control of multiple functions of bionic hand prostheses: Performance and robustness in end users," *Sci. Robot.*, vol. 3, no. 19, p. 3630, Jun. 2018. [Online]. Available: https://www.science.org/doi/10.1126/scirobotics.aat3630

[12] A. Phinyomark and E. Scheme, "EMG pattern recognition in the era of big data and deep learning," *Big Data Cognit. Comput.*, vol. 2, no. 3, p. 21, Aug. 2018. [Online]. Available: https://www.mdpi.com/2504-2289/2/3/21

[13] A. Phinyomark, P. Phukpattaranont, and C. Limsakul, "Feature reduction and selection for EMG signal classification," *Expert Syst. Appl.*, vol. 39, no. 8, pp. 7420–7431, Jun. 2012.

[14] J. M. Hahne et al., "Linear and nonlinear regression techniques for simultaneous and proportional myoelectric control," *IEEE Trans. Neural Syst. Rehabil. Eng.*, vol. 22, no. 2, pp. 269–279, Mar. 2014.

[15] L. J. Hargrove, L. A. Miller, K. Turner, and T. A. Kuiken, "Myoelectric pattern recognition outperforms direct control for transhumeral amputees with targeted muscle reinnervation: A randomized clinical trial," *Sci. Rep.*, vol. 7, no. 1, p. 13840, Oct. 2017. [Online]. Available: https://www.nature.com/articles/s41598-017-14386-w

[16] A. Krasoulis, S. Vijayakumar, and K. Nazarpour, "Multi-grip classification-based prosthesis control with two EMG-IMU sensors," *IEEE Trans. Neural Syst. Rehabil. Eng.*, vol. 28, no. 2, pp. 508–518, Feb. 2020.

[17] A. M. Simon et al., "User performance with a transradial multi-articulating hand prosthesis during pattern recognition and direct control home use," *IEEE Trans. Neural Syst. Rehabil. Eng.*, vol. 31, pp. 271–281, 2023.

[18] Coapt LLC. *Pattern Recognition*. Accessed: Jan. 30, 2026. [Online]. Available: https://coaptengineering.com/pattern-recognition

[19] *MyoPlus System*. Accessed: Jan. 30, 2026. [Online]. Available: https://www.ottobock.com/en-au/Prosthetics/UpperLimbMyoPlus

[20] I. Kyranou, S. Vijayakumar, and M. S. Erden, "Causes of performance degradation in non-invasive electromyographic pattern recognition in upper limb prostheses," *Frontiers Neurorobotics*, vol. 12, Sep. 2018. [Online]. Available: https://www.frontiersin.org/journals/neurorobotics/articles/10.3389/fnbot.2018.00058/full

[21] L. H. Smith, T. A. Kuiken, and L. J. Hargrove, "Evaluation of linear regression simultaneous myoelectric control using intramuscular EMG," *IEEE Trans. Biomed. Eng.*, vol. 63, no. 4, pp. 737–746, Apr. 2016.

[22] J. Zbinden et al., "Improved control of a prosthetic limb by surgically creating electro-neuromuscular constructs with implanted electrodes," *Sci. Transl. Med.*, vol. 15, no. 704, Jul. 2023, Art. no. eabq3665. [Online]. Available: https://www.science.org/doi/10.1126/scitranslmed.abq3665

[23] X. Chen, D. Zhang, and X. Zhu, "Application of a self-enhancing classification method to electromyography pattern recognition for multifunctional prosthesis control," *J. NeuroEng. Rehabil.*, vol. 10, no. 1, p. 44, Dec. 2013.

[24] D. D. Domenico et al., "Long-term upper-limb prosthesis myocontrol via high-density sEMG and incremental learning," *IEEE Robot. Autom. Lett.*, vol. 9, no. 11, pp. 9938–9945, Nov. 2024. [Online]. Available: https://ieeexplore.ieee.org/abstract/document/10654558/?casatoken=RQ8qmgbWwcwAAAAA:5r-PFehidzxQmPXL9yElpQM9znZvWO3aOXl7Trbe25qw39-ACiCZY4E2cc7sOEwsv2rZhPJSCO

[25] M. M.-C. Vidovic, H.-J. Hwang, S. Amsüss, J. M. Hahne, D. Farina, and K.-R. Müller, "Improving the robustness of myoelectric pattern recognition for upper limb prostheses by covariate shift adaptation," *IEEE Trans. Neural Syst. Rehabil. Eng.*, vol. 24, no. 9, pp. 961–970, Sep. 2016.

[26] F. Egle et al., "Preliminary assessment of two simultaneous and proportional myocontrol methods for 3-DoFs prostheses using incremental learning," in *Proc. Int. Conf. Rehabil. Robot. (ICORR)*, Sep. 2023, pp. 1–6.

[27] A. Gijsberts et al., "Stable myoelectric control of a hand prosthesis using non-linear incremental learning," *Frontiers Neurorobotics*, vol. 8, Feb. 2014. [Online]. Available: https://www.frontiersin.org/articles/10.3389/fnbot.2014.00008

[28] M. Nowak, R. M. Bongers, C. K. van der Sluis, A. Albu-Schäffer, and C. Castellini, "Simultaneous assessment and training of an upper-limb amputee using incremental machine-learning-based myocontrol: A single-case experimental design," *J. NeuroEng. Rehabil.*, vol. 20, no. 1, p. 39, Apr. 2023, doi: 10.1186/s12984-023-01171-2.

[29] M. Nowak, I. Vujaklija, A. Sturma, C. Castellini, and D. Farina, "Simultaneous and proportional real-time myocontrol of up to three degrees of freedom of the wrist and hand," *IEEE Trans. Biomed. Eng.*, vol. 70, no. 2, pp. 459–469, Feb. 2023.

[30] A. Gigli, A. Gijsberts, and C. Castellini, "Unsupervised myocontrol of a virtual hand based on a coadaptive abstract motor mapping," in *Proc. Int. Conf. Rehabil. Robot. (ICORR)*, Jul. 2022, pp. 1–6. [Online]. Available: https://ieeexplore.ieee.org/abstract/document/9896414

[31] A. Gigli, A. Gijsberts, M. Nowak, I. Vujaklija, and C. Castellini, "Progressive unsupervised control of myoelectric upper limbs," *J. Neural Eng.*, vol. 20, no. 6, Nov. 2023, Art. no. 066016, doi: 10.1088/1741-2552/ad0754.

[32] D. Yeung, I. M. Guerra, I. Barner-Rasmussen, E. Siponen, D. Farina, and I. Vujaklija, "Co-adaptive control of bionic limbs via unsupervised adaptation of muscle synergies," *IEEE Trans. Biomed. Eng.*, vol. 69, no. 8, pp. 2581–2592, Aug. 2022. [Online]. Available: https://ieeexplore.ieee.org/abstract/document/9712252

[33] E. Campbell, E. Eddy, S. Bateman, U. Côté-Allard, and E. Scheme, "Context-informed incremental learning improves both the performance and resilience of myoelectric control," *J. NeuroEng. Rehabil.*, vol. 21, no. 1, p. 70, May 2024, doi: 10.1186/s12984-024-01355-4.

[34] E. Campbell et al., "(Un)supervised (Co)adaptation via incremental learning for myoelectric control: Motivation, review, and future directions," *IEEE Trans. Neural Syst. Rehabil. Eng.*, vol. 33, pp. 3565–3582, 2025. [Online]. Available: https://ieeexplore.ieee.org/abstract/document/11137388

[35] C. Igual, J. Igual, J. Hahne, and K. Nazarpour, "User-prosthesis coadaptation," in *Control of Prosthetic Hands: Challenges and Emerging Avenues*. U.K.: Institution of Engineering and Technology (IET), 2020, pp. 159–174. [Online]. Available: https://www.research.ed.ac.uk/en/publications/user-prosthesis-coadaptation

[36] J. M. Hahne, S. Dähne, H.-J. Hwang, K.-R. Müller, and L. C. Parra, "Concurrent adaptation of human and machine improves simultaneous and proportional myoelectric control," *IEEE Trans. Neural Syst. Rehabil. Eng.*, vol. 23, no. 4, pp. 618–627, Jul. 2015. [Online]. Available: https://ieeexplore.ieee.org/document/7038151

[37] M. Ortiz-Catalan, F. Rouhani, R. Brånemark, and B. Håkansson, "Offline accuracy: A potentially misleading metric in myoelectric pattern recognition for prosthetic control," in *Proc. 37th Annu. Int. Conf. IEEE Eng. Med. Biol. Soc. (EMBC)*, Aug. 2015, pp. 1140–1143. [Online]. Available: https://ieeexplore.ieee.org/abstract/document/7318567

[38] I. Vujaklija et al., "Translating research on myoelectric control into Clinics—Are the performance assessment methods adequate?," *Frontiers Neurorobotics*, vol. 11, Feb. 2017. [Online]. Available: https://www.frontiersin.org/journals/neurorobotics/articles/10.3389/fnbot.2017.00007/full

[39] P. Kaufmann, K. Englehart, and M. Platzner, "Fluctuating emg signals: Investigating long-term effects of pattern matching algorithms," in *Proc. Annu. Int. Conf. IEEE Eng. Med. Biol.*, Aug. 2010, pp. 6357–6360.

[40] S. M. Wurth and L. J. Hargrove, "A real-time comparison between direct control, sequential pattern recognition control and simultaneous pattern recognition control using a Fitts' law style assessment procedure," *J. NeuroEng. Rehabil.*, vol. 11, no. 1, p. 91, May 2014, doi: 10.1186/1743-0003-11-91.

[41] E. J. Scheme and K. B. Englehart, "Validation of a selective ensemble-based classification scheme for myoelectric control using a three-dimensional Fitts' law test," *IEEE Trans. Neural Syst. Rehabil. Eng.*, vol. 21, no. 4, pp. 616–623, Jul. 2013.

[42] A. M. Simon, L. J. Hargrove, B. A. Lock, and T. A. Kuiken, "Target achievement control test: Evaluating real-time myoelectric pattern-recognition control of multifunctional upper-limb prostheses," *J. Rehabil. Res. Develop.*, vol. 48, no. 6, p. 619, 2011.

[43] L. van Dijk, C. K. van der Sluis, H. W. van Dijk, and R. M. Bongers, "Task-oriented gaming for transfer to prosthesis use," *IEEE Trans. Neural Syst. Rehabil. Eng.*, vol. 24, no. 12, pp. 1384–1394, Dec. 2016. [Online]. Available: https://ieeexplore.ieee.org/abstract/document/7335660

[44] M. B. Kristoffersen, A. W. Franzke, C. K. van der Sluis, A. Murgia, and R. M. Bongers, "Serious gaming to generate separated and consistent EMG patterns in pattern-recognition prosthesis control," *Biomed. Signal Process. Control*, vol. 62, Sep. 2020, Art. no. 102140. [Online]. Available: https://www.sciencedirect.com/science/article/pii/S1746809420302871

[45] A. Boschmann, D. Neuhaus, S. Vogt, C. Kaltschmidt, M. Platzner, and S. Dosen, "Immersive augmented reality system for the training of pattern classification control with a myoelectric prosthesis," *J. NeuroEng. Rehabil.*, vol. 18, no. 1, p. 25, Feb. 2021.

[46] A. Heerschop, C. K. van der Sluis, E. Otten, and R. M. Bongers, "Performance among different types of myocontrolled tasks is not related," *Human Movement Sci.*, vol. 70, Apr. 2020, Art. no. 102592. [Online]. Available: https://linkinghub.elsevier.com/retrieve/pii/S0167945719305536

[47] C. A. Garske, M. Dyson, S. Dupan, G. Morgan, and K. Nazarpour, "Serious games are not serious enough for myoelectric prosthetics," *JMIR Serious Games*, vol. 9, no. 4, Nov. 2021, Art. no. e28079. [Online]. Available: https://games.jmir.org/2021/4/e28079

[48] F. Tessari, J. Hermus, R. Sugimoto-Dimitrova, and N. Hogan, "Brownian processes in human motor control support descending neural velocity commands," *Sci. Rep.*, vol. 14, no. 1, p. 8341, Apr. 2024. [Online]. Available: https://www.nature.com/articles/s41598-024-58380-5

[49] J. A. George et al., "Biomimetic sensory feedback through peripheral nerve stimulation improves dexterous use of a bionic hand," *Sci. Robot.*, vol. 4, no. 32, p. 2352, Jul. 2019. [Online]. Available: https://www.science.org/doi/10.1126/scirobotics.aax2352

[50] J. M. Goodman et al., "Postural representations of the hand in the primate sensorimotor cortex," *Neuron*, vol. 104, no. 5, pp. 1000–1009.e7, Dec. 2019. [Online]. Available: https://linkinghub.elsevier.com/retrieve/pii/S0896627319307779

[51] J. L. Segil and Weir, "Novel postural control algorithm for control of multifunctional myoelectric prosthetic hands," *J. Rehabil. Res. Develop.*, vol. 52, no. 4, p. 449, 2015. [Online]. Available: https://www.ncbi.nlm.nih.gov/pmc/articles/PMC4666529/

[52] N. Jiang, H. Rehbaum, I. Vujaklija, B. Graimann, and D. Farina, "Intuitive, online, simultaneous, and proportional myoelectric control over two degrees-of-freedom in upper limb amputees," *IEEE Trans. Neural Syst. Rehabil. Eng.*, vol. 22, no. 3, pp. 501–510, May 2014. [Online]. Available: https://ieeexplore.ieee.org/abstract/document/6587087

[53] A. Ameri, K. B. Englehart, and P. A. Parker, "A comparison between force and position control strategies in myoelectric prostheses," in *Proc. Annu. Int. Conf. IEEE Eng. Med. Biol. Soc.*, Aug. 2012, pp. 1342–1345. [Online]. Available: https://ieeexplore-ieee-org.biblio.iit.it/document/6346186

[54] A. Ameri, E. J. Scheme, E. N. Kamavuako, K. B. Englehart, and P. A. Parker, "Real-time, simultaneous myoelectric control using force and position-based training paradigms," *IEEE Trans. Biomed. Eng.*, vol. 61, no. 2, pp. 279–287, Feb. 2014. [Online]. Available: https://ieeexplore.ieee.org/document/6600957

[55] J. A. George, T. S. Davis, M. R. Brinton, and G. A. Clark, "Intuitive neuromyoelectric control of a dexterous bionic arm using a modified Kalman filter," *J. Neurosci. Methods*, vol. 330, Jan. 2020, Art. no. 108462.

[56] N. Boccardo et al., "Development of a 2-DoFs actuated wrist for enhancing the dexterity of myoelectric hands," *IEEE Trans. Med. Robot. Bionics*, vol. 6, no. 1, pp. 257–270, Feb. 2024. [Online]. Available: https://ieeexplore.ieee.org/abstract/document/10336883/?casatoken=orbMSkzq9QoAAAAA:UFTOfh8gGPsR3NNR6IZpOaOpDUmxh3s93O8-ogTsnHgwASLO62anz20UGHAbZZ002bSdNw9eDB-lg

[57] M. Laffranchi et al., "The hannes hand prosthesis replicates the key biological properties of the human hand," *Sci. Robot.*, vol. 5, no. 46, p. 0467, Sep. 2020.

[58] H. Braun et al., "Introducing MOSAIC: A modular, open-source suite for assistive intelligent control," *IEEE Access*, vol. 13, pp. 213713–213733, 2025.

[59] A. E. Hoerl and R. W. Kennard, "Ridge regression: Biased estimation for nonorthogonal problems," *Technometrics*, vol. 12, no. 1, pp. 55–67, Feb. 1970.

[60] J. E. Sherman and W. J. Morrison, "Adjustment of an inverse matrix corresponding to a change in one element of a given matrix," *Ann. Math. Statist.*, vol. 21, no. 1, pp. 124–127, Mar. 1950. [Online]. Available: https://projecteuclid.org/journals/annals-of-mathematical-statistics/volume-21/issue-1/Adjustment-of-an-Inverse-Matrix-Corresponding-to-a-Change-in/10.1214/aoms/1177729893.full

[61] S. A. Dalley, H. A. Varol, and M. Goldfarb, "A method for the control of multigrasp myoelectric prosthetic hands," *IEEE Trans. Neural Syst. Rehabil. Eng.*, vol. 20, no. 1, pp. 58–67, Jan. 2012. [Online]. Available: https://www.ncbi.nlm.nih.gov/pmc/articles/PMC3372414/

[62] G. C. Matrone, C. Cipriani, M. Carrozza, and G. Magenes, "Real-time myoelectric control of a multi-fingered hand prosthesis using principal components analysis," *J. NeuroEngineering Rehabil.*, vol. 9, no. 1, p. 40, Jun. 2012, doi: 10.1186/1743-0003-9-40.

[63] S. G. Hart and L. E. Staveland, "Development of NASA-TLX (task load index): Results of empirical and theoretical research," in *Advances in Psychology*, vol. 52, P. A. Hancock and N. Meshkati, Eds., Jan. 1988, pp. 139–183. [Online]. Available: https://www.sciencedirect.com/science/article/pii/S0166411508623869

[64] J. Brooke, "SUS-A quick and dirty usability scale," *Usability Eval. Ind.*, vol. 189, no. 194, pp. 4–7, 1996.